UAV Instrumentation and Computer-Based Controller

Gabriela Martínez-Arredondo[1]* and Ángel Flores-Abad[2]
[1]Instituto Tecnológico de Estudios Superiores de Monterrey
Monterrey, Nuevo León 64830, México. Email: A01042944@itesm.mx
[2]New Mexico State University
Las Cruces, New Mexico 88003, USA. Email: af_abad@nmsu.edu

***Abstract*—In this paper the modeling, instrumentation and a computer-based controller for a mini Unmanned Aerial Vehicle (UAV) is presented. Among the different types of existing UAVs, a Quadrotor is chosen as platform mainly because its geometry is simple and it is easier to achieve an stable flight with it. An own-designed and developed inertial measurement unit (IMU) is used to obtain the angular velocity of the system. Then the nonlinear kinematic equation is derived using the rotation matrix and the Euler angles rate of change. The calibration of the rate gyros is performed by applying the least square method. Based on the rate gyro readings, and the kinematic equations, the 4th order Runge-Kutta method is utilized to obtain the Euler angles. All the algorithms are running in a 32-bit microcontroller and a ground station is employed only to send the speed commands to the controller through wireless communication. For safety, the tests are performed in an also own-designed and built UAV test-stand.**

Keywords: UAV, IMU, calibration, computer-based controller.

I. INTRODUCTION

Since the 1950s the Unites States Army refers to the aircrafts that can fly without a human pilot as UAVs (Unmanned Aerial Vehicles). The UAVs can be controlled either by teleoperation or in a best case autonomously. Last decade several UAVs have been developed because they have some advantages over the manned vehicles. The UAVs consume less fuel, are safety and stable during the flight and can be used to perform dangerous tasks, like accessing places that are difficult or hostile for humans.

Some of the UAV applications are: autonomous field irrigation, natural disasters rescue, aerial assistance in case of fire, weather forecasting, monitoring of pollution levels and traffic density, and mapping. Nowadays research teams all around the world are developing projects in the area of autonomous flying systems, because the numerous applications and the challenges involved. Researches focus mainly in the dynamic modeling (Friis, 2009) ,and in the development of novel control techniques (Bouabdallah, 2007) and motion planning algorithms (Michel, 2010). However most of them use already-developed components, like: IMUs, control units and test facilities. In this work Commercially Off-The-Shelf (COTS) components are used to develop an own designed IMU and controller. The IMU and the controller algorithms are running in the same 32-bit microcontroller, which reduces the space and the weight on the UAV. In order to perform safety experiments, a test stand designed and built by members of our research group is utilized.

The outline of the paper is as follows. In section II the UAV used as platform in this work is described. Section III presents the derivation of the kinematic equations and the Euler angles estimation. Then, section VI introduces the IMU development as well as the rate gyros calibration. Section V describes the experimental results, including a flying test. Finally in section VI conclusions are given.

II. QUADROTOR PLATFORM

A Quadrotor is an aircraft lifted by the force of four rotors mounted in cross configuration. The different maneuvers that a Quadrotor can achieve are done by the variation of the angular velocity of the rotors and thereby the trust and torque from each rotor (Fig. 1). For any fly configuration, the rotors rotate in opposite directions in pairs. Rotors 1 and 3 rotate clockwise and rotors 2 and 4 rotate counter-clockwise. As a result, it is possible to balance the total torque. Depending on the different configurations of the rotors angular velocity, different movements can be performed.

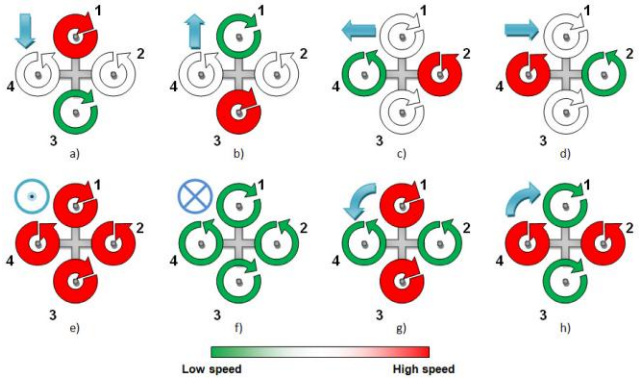

Figure 1. Different Quadrotor maneuvers depending on the speed and direction of the blades rotation

The UAV used here is a Quadrotor GAUI 330X UFO. Fig. 2 shows the platform.

*This work was done while studying at the Universidad Autónoma de Ciudad Juarez

Figure 2. Quadrotor platform GAUI 330X UFO

The main characteristics of the Quadrotor are listed in Table 1.

Table 1: Principal components and characteristics of the Quadrotor GAUI 330X

Parameters	Value/Quantity
Propeller	8 inch / 4
Weight	400 g
Battery	3S Lipo / 1
Electronic Speed Controller (ESC)	10A / 4
Motor	400W-kv 1050 / 4

III. KINEMATIC EQUATIONS

This work is developed as a preliminary stage to achieve autonomous flight. Therefore some variables need to be either measured, calculated or estimated. For any kind of flight control scheme (attitude, hovering or trajectory) at least the angular speed and the Euler angles must be known.

The angular speed of a body can be measured by a rate gyro sensor. However in order to calculate the Euler angles, the kinematic equation must be derived and solved.

1) Coordinate systems

Fig. 3 shows the two coordinate systems used, one is the moving frame called body-frame $B=\{b_x,b_y,b_z\}$, which is attached to the center of mass of the platform. B moves with respect to fixed-frame, here assumed to be the earth frame and labeled world-frame $W=\{n_x,n_y,n_z\}$. When rotating the three axis $x-y-z$, the right hand rule must be held. The body orientation is given by the three Euler angles: ψ, θ and ϕ.

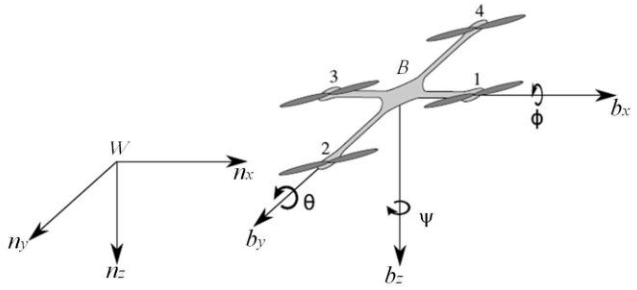

Figure 3. World and body frame

2) Rotation Matrix and Euler angles

A rotation matrix $\mathbf{R}$ is used to perform rotation operations in Euclidian space of a moving frame w.r.t. a fixed frame. Such a rotation is expressed as

$$W=\mathbf{R}\{B\} \qquad (1.1)$$

The most commonly used sets of attitude parameters are the Euler angles. They describe the attitude of the frame B relative to W through three successive rotation angles. The order of the axes about which the reference frame is rotated is important. For example, performing three successive rotations about x-y-z (called 1-2-3) does not yield the same final orientation as rotating in the opposite order z-y-x (3-2-1). The Euler angles are classified according to the order of rotation in :

• Symmetric Set: the first and last rotation axis number is repeated. For example: 3-1-3 set used in astrodynamics to describe the orbit plane.

• Asymmetric Set: no axis rotation number is repeated. For example, the 3-2-1, which is used in vehicle attitude representation as yaw-pitch-roll ($\psi-\theta-\phi$).

Using the 3−2−1 Euler angles, the three principal rotation matrices about z-y-x axis denoted by $\mathbf{R}_\psi,\mathbf{R}_\theta,\mathbf{R}_\phi$ respectively are (referring to Fig. 4):

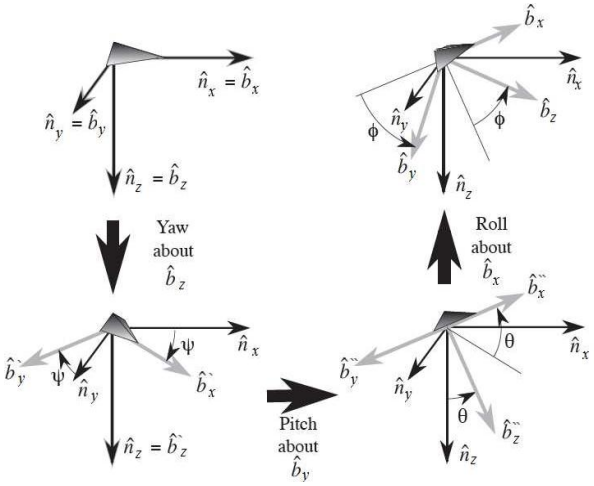

Figure 4. 3-2-1 successive Euler angles rotations

$$\mathbf{R}_{\psi} = \begin{pmatrix} \cos(\psi) & \sin(\psi) & 0 \\ -\sin(\psi) & \cos(\psi) & 0 \\ 0 & 0 & 1 \end{pmatrix} \quad (1.2)$$

$$\mathbf{R}_{\theta} = \begin{pmatrix} \cos(\theta) & 0 & -\sin(\theta) \\ 0 & 1 & 0 \\ \sin(\theta) & 0 & \cos(\theta) \end{pmatrix} \quad (1.3)$$

$$\mathbf{R}_{\phi} = \begin{pmatrix} 1 & 0 & 0 \\ 0 & \cos(\phi) & \sin(\phi) \\ 0 & -\sin(\phi) & \cos(\phi) \end{pmatrix} \quad (1.4)$$

The product of (1.2), (1.3) and (1.4) is given as (1.5) which transforms the orientation of rigid body local frame B to the world frame W .

$$\mathbf{R} = \begin{pmatrix} c\theta c\phi & c\theta s\phi & -s\theta \\ s\psi s\theta c\phi - c\psi s\phi & s\psi s\theta s\phi + c\psi c\phi & s\psi c\theta \\ c\psi s\theta c\phi + s\psi s\phi & c\psi s\theta s\phi - s\psi c\phi & c\psi c\theta \end{pmatrix} \quad (1.5)$$

As mentioned, usually the Euler angles are not measured directly, so that here they will be estimated using the kinematic differential equation that will be derived immediately.

Let the vector $\boldsymbol{\omega} = [\omega_x, \omega_y, \omega_z]^T$ represents the measured angular velocities. By observing Fig. 4, $\boldsymbol{\omega}$ can be written in body frame components as

$$\boldsymbol{\omega} = \omega_x \hat{b}_x + \omega_y \hat{b}_y + \omega_z \hat{b}_z \quad (1.6)$$

and in terms of Euler angles rates as

$$\boldsymbol{\omega} = \dot{\psi}\hat{n}_z + \dot{\theta}\hat{b}'_y + \dot{\phi}\hat{b}_x \quad (1.7)$$

Where

$$\hat{b}'_y = \cos\phi \hat{b}_y - \sin\phi \hat{b}_z$$

$$\hat{n}_z = -\text{in}\,\theta \hat{b}_x + \cos\theta \sin\phi \hat{b}_y + \cos\ \theta \cos\phi \hat{b}_z .$$

After substituting $\hat{b}'_y$ and $\hat{n}_z$ into (1.7) and equating terms with (1.6) the following kinematic equation is found

$$\boldsymbol{\omega} = \begin{pmatrix} \omega_x \\ \omega_y \\ \omega_z \end{pmatrix} = \begin{bmatrix} -\sin\theta & 0 & 1 \\ \cos\theta \sin\phi & \cos\phi & 0 \\ \cos\theta \cos\phi & -\sin\phi & 0 \end{bmatrix} \begin{pmatrix} \dot{\psi} \\ \dot{\theta} \\ \dot{\phi} \end{pmatrix} \quad (1.8)$$

By simple algebraic manipulations of (1.8), the kinematic differential equation for the Euler angles is expressed as

$$\begin{pmatrix} \dot{\psi} \\ \dot{\theta} \\ \dot{\phi} \end{pmatrix} = = \begin{bmatrix} 0 & \sin\phi/\cos\theta & \cos\phi/\cos\theta \\ 0 & \cos\phi & -\sin\phi \\ 1 & \tan\theta\sin\phi & \tan\theta\cos\phi \end{bmatrix} \begin{pmatrix} \omega_x \\ \omega_y \\ \omega_z \end{pmatrix} \quad (1.9)$$

Although from (1.9) it can be noticed that this set of angles presents singularities at $\pm 90^{\circ}$ in the pitch angle, this is not a big concern if it is considered that the Quadrotor maneuvers are usually far from that orientation. In order to solve the ODE system (1.9) a 4th order Runge-Kutta algorithm is computed in real time, using a step size of $h = 0.1$

IV. Instrumentation: Sensors and Actuators

The IMU used in this work was previously designed by members of our research team (Hatamleh, et al., 2011). This IMU was created with the purpose of providing a new method to measure angular acceleration without calculating the time derivative of the angular velocity. Nevertheless, the Euler angles were assumed known. Here the Euler angles are obtained by solving equation 1.9. Even though the IMU used here is based in the previous design, a more efficient accommodation of the components were required. As a result, the IMU is smaller (Fig. 5) and can be installed on the top of the Quadrotor. Furthermore all the components are surface mounted devices (SMD) being less susceptible of misalignment and tilting errors.

Fig. 6 shows the allocation of the IMU components. This board consists of: one PIC32MX440, three 3-axis accelerometers, one XY-axis gryo, Z-axis gyro, one microSD card, two programmable LEDs and several buttons.

For this application only the rate gyros are used to measure the angular velocity and to estimate the Euler angles. The data acquisition period is of 100 ms through 10 bits of analog to digital conversion.

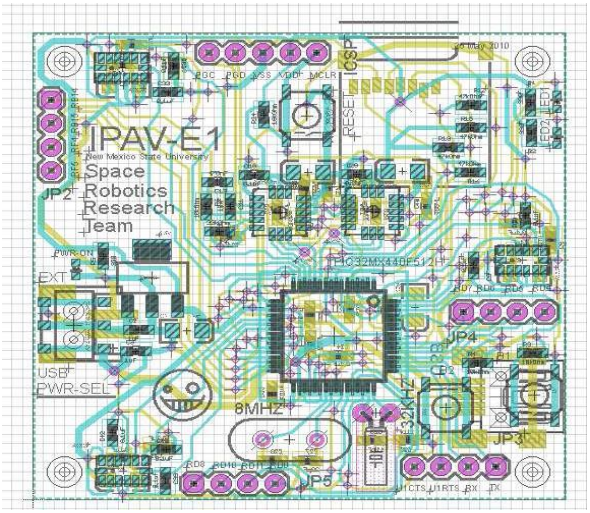

Figure 5. IMU design for reduced space & payload applications

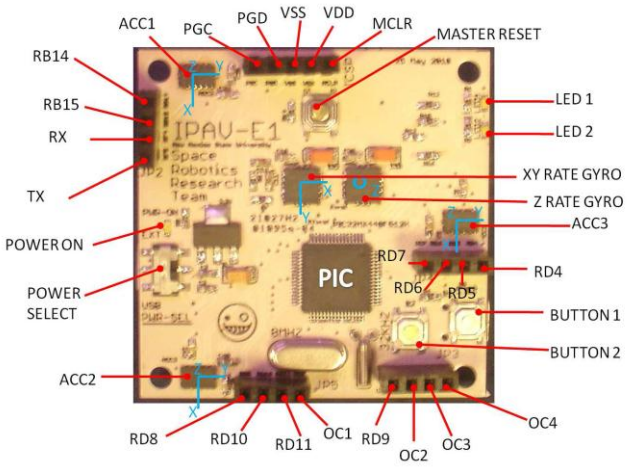

Figure 6. Components of the IMU

1) Rate gyros calibration

The controlled rotating table (CRT) showed in Fig. 7 is used to get a reference angular speed for the calibration process. The Speed of the CRT is controlled by means of a PID controller implemented in MatLab/Simulink®. Fig. 8 shows the Simulink® block diagram, where the reference speed is the desired angular speed of the CRT and motor shaft´s angular speed is the fed back signal. A Quanser® data acquisition board is used to send the control signal to a amplifier module, which drives the DC motor that makes the table rotate.

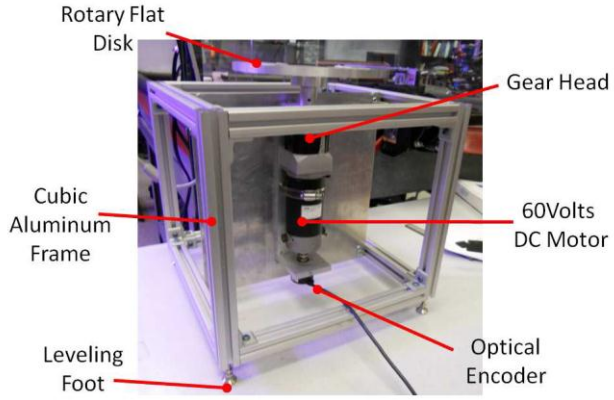

Figure 7. IMU calibration platform

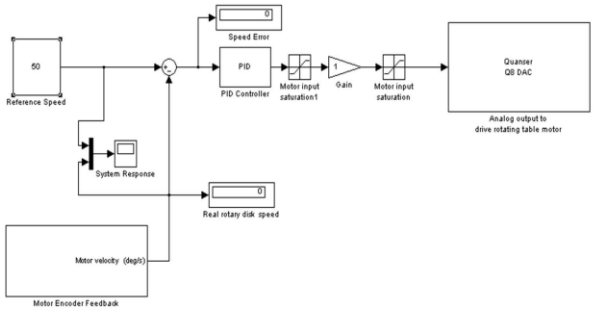

Figure 8. Simulink® block diagram for the PID controller of the CRT

During each experiment the table is rotated from 0 to 50 deg/s with increments of 5 deg/s. Fig. 9 shows the rate gyros orientation of each axis. Fig. 9a, 9b and 9c corresponds to the x, y and z axis, respectively.

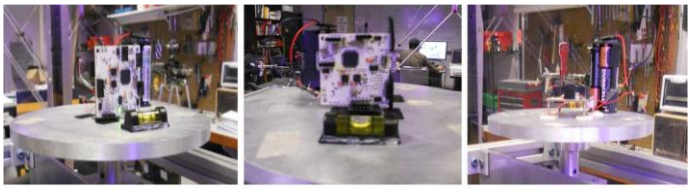

Figure 9. IMU rotations to calibrate each rate gyro, a) for the x-axis, b) for the y-axis and c) for the z-axis

Throughout the rate gyro calibration process, the sensors showed a linear performance. Therefore, the least square method is used to approximate each real sensor reading to the ideal sensor reading. In the basic equation of a line $y = mx + b$, m is represented by the sensitivity factor and b by the bias. Using Gaussian elimination for solving the resulting system of linear equations, we get:

$$y_{\omega x} = 0.64x + 0.273 \qquad (1.10)$$

$$y_{\omega y} = 0.63x - 0.090 \qquad (1.11)$$

$$y_{\omega z} = 0.627x + 9.045 \qquad (1.12)$$

Now, the equations (1.10) (1.11) and (1.12) are normalized to set the origin at zero. The bias must be subtracted from each sensor reading and then, the result is multiplied by the sensitivity factor. The equations (1.13) (1.14) and (1.15) show the normalized sensor data relations.

$$\text{gyro}(\omega x) = 1.5625(\text{sensor}_{\text{read}} - 0.273) \qquad (1.13)$$

$$\text{gyro}(\omega y) = 1.5625(\text{sensor}_{\text{read}} + 0.0909) \qquad (1.14)$$

$$\text{gyro}(\omega z) = 1.6129(\text{sensor}_{\text{read}} - 9.0454) \qquad (1.15)$$

2) Brushless DC motors characterization

Each rotor has an angular speed ω_i and produces a vertical force F_i according to the equation

$$F_i = k_F \omega_i^2 \qquad (1.16)$$

Therefore, the necessary total force to hover the Quadrotor is related to the total weight of the platform. The total force is divided in the four motors to get

$$F_i = \frac{mg}{4} \qquad (1.17)$$

The relation between the input voltage to the motor and the matching speed of rotation is given by $\omega_i = 1050\text{rpm}/\text{Input(Volts)}$.

In order to obtain the real duty cycle range that permits the control of the brushless DC motors, an experimental characterization was performed. For this procedure, the control unit generates the Pulse Width Modulation (PWM) signal to activate an electronic speed control (ESC) that drives the brushless DC motor at the desired angular speed.

The ESC works with a nominal PWM signal of 50 Hz with a minimum and maximum duty cycle of 5% and 10% respectively. The motors speed variation per volt, is also known as 1050rpm/volt. Then using this nominal values, it is possible to establish the real limits for each motor by testing its duty cycle and the corresponding rpm. Table 2 shows the real performance for each rotor of the platform, the minimum require duty cycle signal to lift the Quadrotor and the maximum duty cycle of each motor.

Table 2: Real motor performance

	Min			
Motor	**PWM**	**Vrms (mV)**	**rpm**	**°/s**
1	5.40%	750	787.5	4725
2	5.40%	755	792.8	4757
3	5.50%	770	808.5	4851
4	6.00%	796	835.8	5015
	Max			
Motor	**PWM**	**Vrms (mV)**	**rpm**	**°/s**
1	7.60%	898	942.9	5657
2	7.60%	899	944	5664
3	7.60%	904	949.2	5695
4	7.60%	900	945	5670

V. TEST RESULTS

1) Rate gyros calibration

The results of the three rate gyros calibration are depicted in Fig. 10. The real sensor readings before calibration are shown with squares, which behavior is mostly linear. A dashed line indicates the desired sensor linearization. The circles correspond to the sensors reading after the calibration process, and the solid line represents the desired one. As it can be observed, the calibration is correct, because the desired and the calibrated readings are almost the same at each measured point.

Once the calibration has been performed successfully, two experiments are done. The first one is to set the zero of each sensor and the second one to verify the accuracy of the sensors measurements.

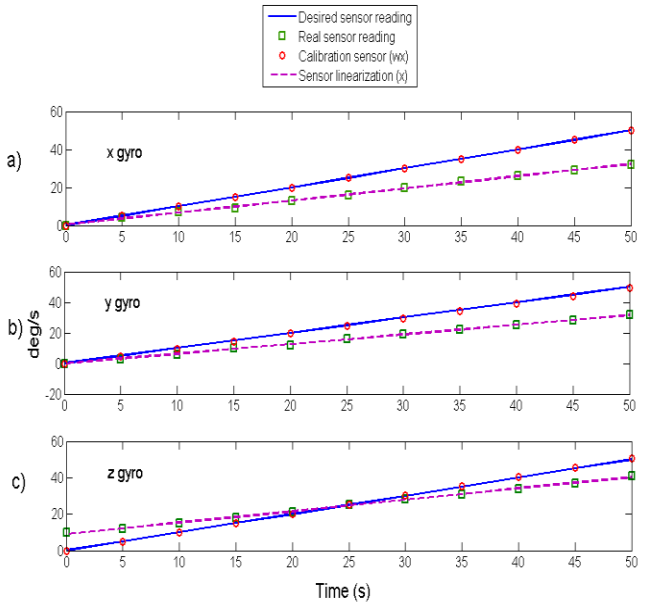

Figure 10. Rate gyros performance during the calibration process

In the first experiment, the angular velocity of the CRT is set at 50 deg/s until 40 s, then it is stopped (0 deg/s). The desired and the measured angular velocities are compared in Fig. 11. As it can be noticed, they are very close to each other.

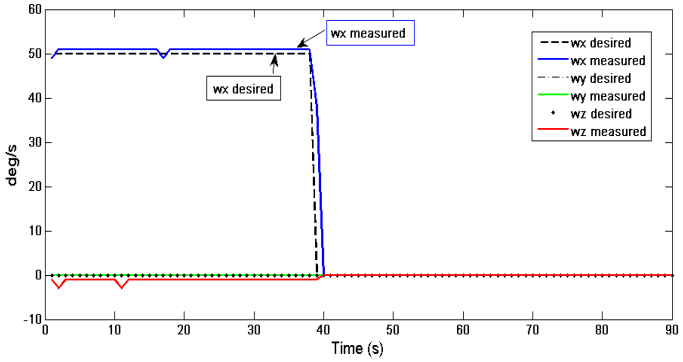

Figure 11. Comparison between the simulated and measured angular velocity ω_x.

In the second experiment the CRT is rotated at a constant angular velocity for ≈ 38 s, causing the angle ϕ changes in a ramp shape. Then when the rotating table is stopped, ϕ remain constant as shown in Fig. 12.

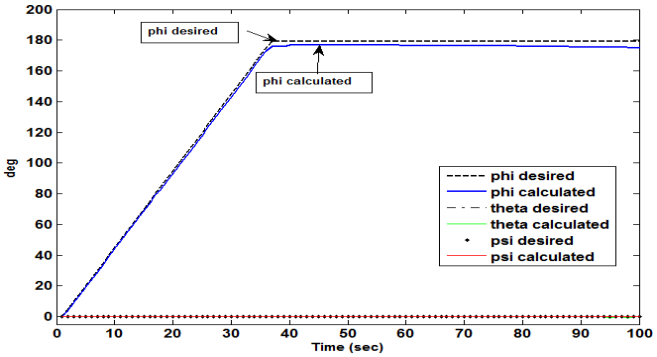

Figure 12. Comparison between the simulated and the calculated ϕ Euler angle

2) Safety Real Flying Test

Fig. 13 shows the components of the system and the sequence of the signal during the test. As mentioned before, the IMU and the controller unit are in the same board. The ground station is conformed by a Laptop and the transmitter Xbee module. This station is useful to set up the motors, increase or decrease the motors velocity and turn on/off the system. The Xbee addressing is also done in the ground station. Once the modules are ready, it is possible to send user-specified characters to turn on the system. Then, the control unit sends the PWM signal to the ESC, which provide the necessary voltage and current to activate the motors. Finally the blades attached to the motors' shaft give the airborne forces to the aircraft.

.

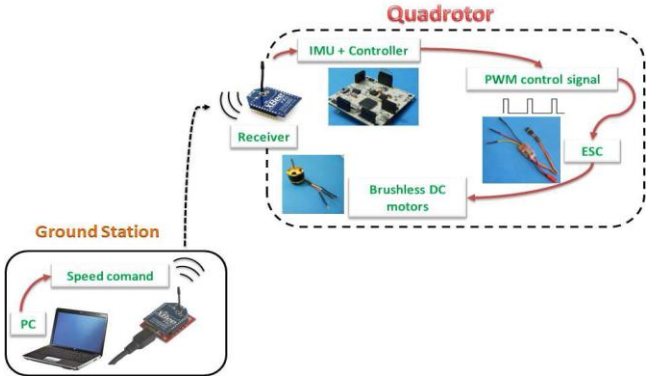

Figure 13. Block diagram for the open loop flying test

An indoors experiment using a safety test stand, designed and built for our research team (Qi, et al. 2008) was performed to verify the study in a real situation. Fig. 14 shows the Quadrotor mounted on the test stand while it is flying according to the speed commands sent from the computer through wireless communication.

Figure 14. Quadrotor in a safety flying experiment on the test stand.

VI. CONCLUSIONS

This paper described the modeling, instrumentation and computer-based controller of a Quadrotor. A previously designed IMU was modified and developed for this application using COTS components. The kinematic equations were derived using Newton-Euler principles. Based on those equations and the rate gyros readings, the Euler angles were obtained using a 4th Order Runge-Kutta algorithm. The rate gyros calibration process applying the least square method is described. To validate the approach, a real flying experiment was performed in a safety test stand. As a preliminary step in the development of an autonomous controller, a computer was used to send the speed commands instead of the radio controller.

VII. ACKNOWLEDGMENTS

The authors would like to thank to Dr. Ou Ma of NMSU for allowing us to use the mechatronics lab and all the facilities necessary for the development of this work. As well, PhD Students Pu Xie and Khaled Hatamleh for all their technical help and suggestions.

REFERENCES

Ollero Baturone, A. (2007). *Robótica: Manipuladores y robots móviles* : Alfaomega.

Bouabdallah, S., Murrieri, P., Siegwart, R (2004). Design and Control of an Indoor MicroQuadrotor. *IEEE International Conference on Robotics and Automation.* New Orleans, USA. pp.4393-4398.

Bouabdallah, S., Siegwart, R (2007). Full Control of a Quadrotor. *IEEE conference on Intelligent Robots and system.* San Diego, USA. pp.153-158.

Brito, J. 2009. *Quadrotor prototype*. Master thesis, Universidad Tecnica de Lisboa, Portugal.

Hatamleh, K., Ma, O., Flores-Abad, A., Xie, P. Development of a Special Inertial Measurement Unit for UAV Applications. *ASME Journal of Dynamic Systems Measurement and Control*, 2011 (accepted).

Friis, J., Nielsen, E., Foldager, R (2009). *Autonomous Landing on a Moving Platform*. Technical report. Aalborg University, Denmark.

Hibbeler, R (2004). *Engineering Mechanics: Dynamics*: Prentice Hall.

Pitman, D. (2010) *Collaborative Micro Aerial Vehicle Exploration of Outdoor Environments*. Master Thesis. Massachusets Institute of Technology.

Schaub, H., Junkins, J.(2009). *Analytical Mechanics of Space Systems* : AIAA Education Series.

Michael, N., Mellinger, D., Lindsey, Q., Kumar, V. (2010) The GRASP Multiple Micro-UAV Test Bed. *IEEE Robotics and Automation Magazine*, Issue:3. pp. 56-65.

Qi, L. Ortega, C and Ma, O. (2008). A gravity balanced test stand for flight testing of small/micro unmanned aerial vehicles. *ASME International Mechanical Engineering Congress and Exposition*. Boston, MA. USA. pp. 41-47.